

# Constructing the Coronal Magnetic Field

*By Correlating Parameterized Magnetic Field Lines  
With Observed Coronal Plasma Structures*

G. Allen Gary \*

*Space Science Laboratory/ES82  
NASA/Marshall Space Flight Center, AL 35812, U.S.A.*

David Alexander †

*Lockheed Martin Solar and Astrophysics Lab, Org. H1-12 B/252  
3251 Hanover St., Palo Alto, CA 94304, U.S.A.*

(Received ..... ; Accepted in final form .....)

**Abstract.** A method is presented for constructing the coronal magnetic field from photospheric magnetograms and observed coronal loops. A set of magnetic field lines generated from magnetogram data is parameterized and then deformed by varying the parameterized values. The coronal flux tubes associated with this field are adjusted until the correlation between the field lines and the observed coronal loops is maximized. A mathematical formulation is described which ensures that (i) the normal component of the photospheric field remains unchanged, (ii) the field is given in the entire corona over an active region, (iii) the field remains divergence free, and (iv) electric currents are introduced into the field. It is demonstrated that a parameterization of a potential field, comprising a radial stretching of the field, can provide a match for a simple bipolar active region, AR 7999, which crossed the central meridian on 1996 Nov 26. The result is a non-force-free magnetic field with the Lorentz force being of the order of  $10^{-5.5}$  gm cm s<sup>-2</sup> resulting from an electric current density of  $0.079 \mu\text{A}/\text{m}^2$ . Calculations show that the plasma beta becomes larger than unity at a relatively low height of  $\sim 0.25 r_{\odot}$  supporting the non-force free conclusion. The presence of such strong non-radial currents requires large transverse pressure gradients to maintain a magnetostatic atmosphere, required by the relatively persistent nature of the coronal structures observed in AR 7999. This scheme, is an important tool in generating a magnetic field solution consistent with the coronal flux tube observations and the observed photospheric magnetic field.

**Key words:** Solar: Coronal Loops, Solar: Magnetic Fields, Solar: X-Rays

**Abbreviations:** MSFC – Marshall Space Flight Center

---

\* E-mail: allen.gary@msfc.nasa.gov

† E-mail: alexander@lmsal.com

## 1. Introduction

The Sun's corona is dominated by magnetic field. This magnetic field serves to confine coronal plasma to predominantly linear structures or loops, the emission of which is pre-eminent in X-ray or EUV images (e.g. Acton, 1996; Rosner, Tucker and Vaiana, 1978). The photospheric and coronal magnetic field also plays a critical role in the heating and dynamics of the confined plasma, resulting in transient phenomena such as prominence eruptions, coronal mass ejections and flares. Despite the overwhelming agreement that the field dominates in the low corona, all evidence for this contention is generally inferred from the form of the plasma emission, since no direct measure of the coronal field can yet be made (cf. White and Kundu, 1997).

A standard approach to determining the coronal field is the extrapolation of the observed field at the surface into the corona via various assumptions about the possible nature of the field, e.g. current-free or force-free (Sakurai, 1981; Amari et al., 1997). This approach allows one to generate an approximation to the coronal distribution of magnetic field which can then be compared with the observed distribution of the plasma as determined from EUV and X-ray observations (cf. Jiao, Mclymont and Mikić, 1997). While apparently straightforward and reasonably successful, the extrapolation techniques are subject to

numerous difficulties which are as yet not fully resolved (see Amari et al., 1997).

In particular, the general magnetic field associated with an active region cannot be obtained since there is no closed form solution for the non-force-free, magnetohydrodynamic problem. This difficulty in modeling the magnetic field is imposed in part by the fact that the magnetic field lines originate in a high-beta plasma region,  $\beta > 1$ , in the granular and inter-granular photosphere and traverse a low-beta region,  $\beta \ll 1$ , in loop structures in the low corona, to culminate once more in a large-scale  $\beta \geq 1$  region in the solar wind. While there has been a number of current-free and force-free numerical models which attempt to extrapolate the magnetic field from the photosphere, the problem is generally ill-posed and assumes  $\beta \ll 1$  (Sakurai, 1989; Gary, 1990; McClymont, Jiao, and Mikić, 1997). In addition, the upper boundary conditions required to make the problem tractable and well-posed are essentially unknown. Consequently, a number of approximate solutions and numerical methods have been devised each with its own strengths and weaknesses.

One such assumption is the inclusion of a *source surface* which mimics the effect of the,  $\beta \geq 1$ , solar wind by forcing the field to be radial beyond a certain radius,  $r = r_s$ . This approach was first introduced by Altschuler and Newkirk (1969) and Schatten, Wilcox and Ness (1969)

and has since been used by many authors (e.g. Levine, Schulz and Frazier, 1982; Sakurai, 1993; Zhao and Hoeksema, 1995). As an example, in potential field models, applying the source-surface assumption allows a spherical potential solution to be derived using the appropriate Green's function  $G(r, r')$  and the observed line-of-sight field,  $B_p$  (Sakurai, 1993). In this case the coronal magnetic field is given by

$$\mathbf{B}(\mathbf{r}') = \nabla\Phi(r) = \nabla \left[ \int_S G(r, r') B_p(r') ds' \right] \quad (1)$$

However, it should be noted that in Sakurai's approach, where  $G(r, r')$  is given by a truncated series, the vector field at the source surface is only approximately radial for a closed-form Green solution.

The general application of a source surface induces a radial stretching of the field lines as compared to a set of potential field lines with the effect that the stretching depends on the height of the source surface,  $r_s$ , chosen to be spherical in most formulations. The motivation for the present work comes, in part, from the inability of the source surface models to provide the necessary modification of the magnetic field to reproduce the observed coronal structures. Specifically, a more direct transformation is required to provide sufficient radial extensions of the field. An alternative approach would be the application of a more general, e.g. non-spherical, source surface which has proved successful in

simulating the expected physical consequences of coronal MHD effects in the large-scale coronal field (Levine et al., 1982). However, the inclusion of such a source surface has severe implications for the form of the global field and it is not clear if these can be made self-consistent with the local effects required to simulate an active region.

The application of a source-surface or some other means of modifying the field in lieu of considering the actual MHD equations, while mathematically convenient and providing a magnetic field solution, cannot fully address the nature of the problem. The solar wind is a region of high-beta plasma and the transition from the low-beta corona to this region is generally more complex than the simple, single radial shell imposed by the source-surface models. The inclusion of magnetohydrodynamic effects is clearly an important consideration in the modeling of the solar corona, particularly for the large-scale structures seen in white-light: this is beautifully illustrated by the MHD model of Pneuman and Kopp (1971) which incorporates the interaction of field and plasma as the coronal material expands out into interplanetary space. Consequently, a general solution would require full use of the MHD equations to address the form of the field in the various beta regions (see Mikić, Barnes, and Schnack, 1988; Jiao et al., 1997; Amari et al., 1997). The limiting factor in deriving fully three-dimensional MHD solutions is the significant amount of computational

effort required as well as the need to include all the necessary magnetic and hydrodynamic boundary conditions (cf. Antiochos and Dahlburg, 1997).

Most of these studies have concentrated on modeling the corona on large scales, reproducing the general shape of the streamer belt during solar minimum conditions. However, observations from the *Yohkoh* spacecraft have shown that the typical field configuration displayed by the helmet streamer, a closed field region surrounded by open field with a cusp/current sheet as the interface between the two, has also been observed on smaller scales in active region structures (e.g. Tsuneta, 1996), suggesting a similarity in the distribution of currents and field on these very different scales. Such a configuration on the scales of active regions is not easily addressed by a source surface approach which is restricted by the form of the global coronal field. The objective of the work presented here is to investigate the interaction between the active region field and the plasma it contains, by reconstructing the coronal field using a novel approach which introduces a radial transformation of the field without resorting to a source surface or computationally intensive MHD calculations.

We determine the coronal distribution of the field by modifying an initially simple configuration to produce a distribution which matches the observed coronal loops. The coronal magnetic field is reconstruct-

ed via a transformation procedure in which an initially current-free distribution of magnetic field lines is deformed by performing a radial stretching at each point of the field. Assuming the magnetic field to be traced by the coronal emission, the field lines are ‘stretched’ until the correlation between them and the observed coronal loops is maximized. In essence, we are perturbing an initially derived potential field subject to the constraints that the three-dimensional coronal field is given by the distribution of X-ray emitting plasma. The form of the field generated in this way requires the presence of cross-field currents in the corona to reproduce the observed active region structure. This indicates that magnetic field energy (derived from the line-of-sight field only) is not sufficient to produce the active region corona.

The radial stretching transformation used here is directly analogous to that used in the magnetostatic models of the large-scale corona (see Bogdan and Low, 1986) and consequently several implications from these models can be applied. The use of such a transformation in magnetic field reconstructions of active regions is, we believe, new and yields a number of interesting consequences.

The role of the cross-field currents in heating the corona and their implications not only for producing the observed active region morphology but also for increasing the free energy available for release in

transient phenomena, provide further impetus to the present investigation (cf. Wolfson and Dlamini, 1997).

We introduce our transformation method in section 2 and apply it to the case of AR 7999 in section 3. The results are interpreted in section 4 where we discuss the implications of the inferred non-radial currents. The correlation method between the theoretical and observed coronal field is given in Appendix A, while the magnitude of the inferred currents is calculated in Appendix B. Our conclusions are presented in section 5.

## 2. Transformation of the Magnetic Field

The analysis proposed here is based on a transformation method which assumes : (1) the conservation of magnetic flux  $\nabla \cdot \mathbf{B} = 0$ , (2) an invariant photospheric vertical magnetic field, i.e., the observed radial boundary condition  $B_r(r = r_\odot)$  is unchanged, (3) the initial configuration is a known (potential) field,  $\nabla \cdot \mathbf{B} = 0$  and  $\nabla \times \mathbf{B} = 0$ , i.e., the unperturbed, unstretched, zero-order field, (4) a transformation is performed which radially stretches the field lines ( $F_i$ ,  $i \subset$  all field lines), and simulates possible MHD effects in a simple analytic variation of only one of the spherical coordinates.  $F_i$  represents the locus of the points which define the  $i^{th}$  field line.



The point-by-point spatial transformation  $T_K$  of the field lines is given by

$$T_K\{F_i[r, \theta, \phi]\} = F_i[k(r - r_\odot) + r_\odot, \theta, \phi] \quad (2)$$

which is a function of the height,  $h = r - r_\odot$ , and the constant radial stretching factor  $k$ . Using this transformation from the potential field ( $\mathbf{B}$ ) and  $\nabla \cdot \mathbf{B} = \nabla \cdot \mathbf{B}' = 0$ , the resulting magnetic field ( $\mathbf{B}'$ ) can be shown to be

$$B'_r = w(r, r_\odot, k)B_r, \quad (3)$$

$$B'_\phi = v(r, r_\odot, k)B_\phi, \quad (4)$$

$$B'_\theta = v(r, r_\odot, k)B_\theta, \quad (5)$$

where

$$w(r) = \frac{[h + r_\odot]^2}{[kh + r_\odot]^2} \quad \text{and} \quad v(r) = \frac{h + r_\odot}{k[kh + r_\odot]}. \quad (6)$$

The parameter  $k = 1$  implies no stretching, and  $k > 1$  implies an increasing field stretching as  $r$  increases. However, we emphasize that at  $r = r_\odot$  ( $h = 0$ ) the radial component of the photospheric field is recovered unchanged for all values of  $k$ . A similar ‘stretching’ transformation was introduced in modeling the large-scale corona above helmet

streamers (e.g. Bogdan and Low, 1986; Gibson and Bagenal, 1995). Gibson and Low (1998) have recently utilized a generalized radial solution for stretching the magnetic field in the modeling of CMEs. This generalized solution invokes a coordinate transformation such that  $r \rightarrow kr + a$  where  $k$  and  $a$  are arbitrary constants (Gibson and Low choose  $k = 1$  without loss of generality). Such a transformation was required for the magnetic field to satisfy the magnetostatic equations. This transformation is equivalent to that shown in equation (2) with  $a = -(k-1)r_\odot$  and  $k \geq 1$ , although in the form adopted by Gibson and Low it becomes a translational coordinate transform rather than the rescaling transform adopted here.

The electric currents induced by the stretching of the magnetic field are easily determined from

$$\begin{aligned}
\mathbf{J}(r, \theta, \phi) &= \nabla \times \mathbf{B}' \\
&= \frac{1}{r \sin \phi} \left[ \frac{\partial}{\partial \phi} (B'_\theta \sin \phi) - \frac{\partial}{\partial \theta} (B'_\phi) \right] \hat{\mathbf{u}}_r \\
&\quad + \frac{1}{r} \left[ \frac{1}{\sin \phi} \frac{\partial}{\partial \theta} (B'_r) - \frac{\partial}{\partial r} (r B'_\theta) \right] \hat{\mathbf{u}}_\phi \\
&\quad + \frac{1}{r} \left[ \frac{\partial}{\partial r} (r B'_\phi) - \frac{\partial}{\partial \phi} (B'_r) \right] \hat{\mathbf{u}}_\theta, \tag{7}
\end{aligned}$$

which are orthogonal to the radial direction, since, the coefficient of  $\hat{\mathbf{u}}_r$ ,

$$\left[ \frac{\partial}{\partial \phi} (v(r) B_\theta \sin \phi) - \frac{\partial}{\partial \theta} (v(r) B_\phi) \right] = 0. \tag{8}$$

These cross-field currents represent the physical mechanism which produces the three-dimensional distribution of the magnetic field required to match the observed active region morphology. The inferred presence of these non-radial currents have strong implications for the force balance in the active region corona. The magnitude of these currents and their corresponding Lorentz forces will be considered in section 4.

### 3. Data Analysis: Active Region 7999

The physical cynosure for this study, is the active region AR 7999. This region has the following desirable properties: (1) the photospheric magnetic field is a relatively simple bipolar configuration, (2) the region is at a slow evolutionary phase when observed at central meridian passage, (3) it is the *only* active region in the observed hemisphere, (4) there is a large data set including the observed coronal loops from *Yohkoh*/SXT and SOHO/EIT instruments.

An SXT image of AR 7999 as it crossed the Central Meridian on 1996 Nov 26 21:48:18 UT is shown in Figure 1. One can see that the active region is compact and exhibits a relatively simple bipolar structure. Each frame of Figure 1 shows the same soft X-ray image. A comparison between the extrapolated field lines and the soft X-ray loops clearly demonstrates that a potential field ( $k = 1$ ) does not adequately

reproduce the observed structure. The field lines were generated from the spherical potential code of Sakurai (1981; 1982) using photospheric field data from a KPNO magnetogram taken at 18:05:16 UT. The field lines have been rotated to coincide with the time of the soft X-ray image and a heliographic grid ( $10 \times 10$  degrees) has been superposed to show the location and size of the image. As the stretching parameter,  $k$ , is increased, the match to the observed X-ray structure improves. It is apparent from Figure 1 that a stretching factor of  $k \approx 3$  best approximates the distribution of coronal loops. In Appendix A, we derive the best fit to be  $k = 3.4$ . Even though we do not have a stereoscopic view to establish that the field lines are consistent in height with the coronal loops, we can use the solar rotation with the same field lines to establish the credibility of the correlation. The results of field lines for the succeeding days are shown in Figure 2.

Therefore, by these correlations, it is seen that the radial stretching of the field lines provide a significant improvement in matching the soft X-ray flux tubes for this active region. We have provided a visual comparison of the effect and numerical verification of the improvement. In the next section we will interpret this important finding.

#### 4. Interpretation of the Radially Stretched Field Lines

##### *Field-Plasma Connection*

We can estimate whether a linear stretching factor of  $\sim 3$  is reasonable by comparing with the results of MHD models. Pneuman and Kopp (1971) developed a numerical MHD model of the large-scale corona to describe the interaction between the magnetic field and coronal plasma in the development of a helmet streamer. The application of this model results in a radial stretching of the field as compared to a potential field and the formation of a current sheet. Using Figure 8 of Pneuman and Kopp (1971), we can estimate the spatial stretch imposed by their numerical MHD model. In the height range,  $r = 1.2 - 1.8 r_{\odot}$ , the corresponding radial stretching factors would be  $k = 1.1 - 4.4$ ; similar to the results obtained from Figure 1. The MHD results of Pneuman and Kopp (1971) do not provide for a large degree of radial stretching close to the solar surface ( $h \simeq 0-0.5 r_{\odot}$ ) as required by the active region studied here. However, they were not concerned with the detailed modeling of the corona on active region scales, adopting an essentially potential field distribution low in the corona. In order to produce the required radial stretching in the active regions while maintaining the large-scale coronal geometry, a much more complex interaction between the plasma and the magnetic field is necessary.

Cusped loops are widespread, seem to have several different manifestations, and have been observed at heights of  $\sim 0.2 r_{\odot}$  which give further evidence for the influence of MHD effects at heights considerably lower than previously considered (Hiei and Hundhausen 1996; Strong 1994). These observations all imply a departure from the classical potential field model and, consequently, stress the importance of currents in the corona.

From the Pneuman and Kopp (1971) results, at  $r = 1.8 r_{\odot}$ , the plasma beta can be estimated to be  $\beta \simeq 35 - 50$ , and hence far from any force-free approximation (Suess, 1998), indicating the probability that cross-field currents exist in the large-scale coronal field. Lower in the corona one expects the plasma beta to be very much less than unity. This is not always true for active regions, however. In the outer bright loops of a large active region, an estimate of the plasma beta can be determined via

$$\beta = \frac{\text{plasma pressure}}{\text{magnetic pressure}} = \frac{16\pi nkT}{B^2} \simeq 0.07 \frac{n_9 T_6}{B_{10}^2}. \quad (9)$$

where  $B_{10} \equiv B/10 \text{ G}$ ,  $n_9 \equiv n/10^9 \text{ cm}^{-3}$ , and  $T_6 \equiv T/10^6 \text{ K}$ . For reasonable active region parameters,  $[B_{10} = 1, n_9 = 1, T_6 = 3]$ ,  $\beta \simeq 0.2$ . Thus, for a typical active region, we expect that the gas pressure is not completely ignorable. In Figure 3 we show the magnitude of the

magnetic field strength along the potential field lines ( $k = 1$ ) as a function of height. This shows that at few tenths of  $r_{\odot}$  the magnetic field does indeed fall below 10G.

Secondly, using the form of the magnetic field with height shown in Figure 3 in the case of AR 7999 we can estimate the plasma beta at each point in the active region. To do this we consider the active region when it was at the West limb (1996 Dec 2) and determine the emission measure and temperature from the *Yohkoh*/SXT using a filter-ratio technique (see Hara et al., 1992). This was done by first summing 34 images in each of the two thin filters of the SXT to provide a single summed image pair (the images were co-registered and corrected for background before summing; see Alexander, 1998). For each image in the image pair, active region pixels lying along the arc defined by a given height above the limb were summed and the ratio of the two filters taken to provide an average temperature and emission measure for the active region at that height. The density is then determined from the emission measure assuming a line-of-sight depth of  $2.5 \times 10^4$  km, i.e.  $n = \sqrt{EM/Al}$  where  $A$  is the area of an SXT pixel ( $1.9 \times 10^7$  km<sup>2</sup>). Armed with the average density, temperature and magnetic field variation with height we determined the plasma beta variation shown in Figure 4. The plasma beta reaches unity at a height  $\sim 1.75 \times 10^5$  km or  $\sim 0.25 r_{\odot}$ .

*Electric Currents in the Corona*

The modification of the coronal magnetic field distribution necessary to support this active region configuration requires the presence of a coronal electric current system. An approximation to the magnitude of the induced electric currents can be made from equation (7) by assuming that the spherical coordinate system locally can be replaced by a Cartesian coordinate system (see Appendix B). This approximation yields the  $\phi$ -component of the electric current as  $J_\phi \sim 0.079 \mu\text{A m}^{-2}$  at  $z \sim 0.2r_\odot$ . The magnitude of this current is comparable to that found in magnetostatic models of the large-scale corona (e.g. Bagenal and Gibson, 1991), where typical coronal current densities of order  $0.02 \mu\text{A m}^{-2}$  are found at heights,  $h \sim 0.1 - 0.3 r_\odot$ . The geometry assumed in the large-scale coronal models is relatively simple, especially at low heights with assumed field strengths  $\sim 1$  G and so we should not expect the conditions to be too similar to the active regions being modeled here. However, these models and our results indicate that large coronal current densities are a common feature of the corona.

A simple calculation will show that these electric currents are somewhat high compared to the pressure force required for coronal force balance, where the electric currents are on the order of  $0.001 \mu\text{A m}^{-2}$ . This can be seen by deriving the equivalent electric current corresponding to the radial pressure gradient. Assume the radial component of



the pressure gradients is balanced by the gravity force at  $r = 1.2r_\odot$  ( $z = 0.2r_\odot$ ):

$$\left| \frac{dp}{dr} \right| \sim \rho g = (m_p n) g_{surf} \left( \frac{r}{r_\odot} \right)^{-2} \simeq 3.2 \times 10^{-11} n_9 \text{ erg cm}^{-4}. \quad (10)$$

where  $g_{surf} = 2.74 \times 10^4 \text{ cm s}^{-2}$  is the gravitational acceleration at the surface of the Sun. Then let the Lorentz force per unit mass for a current density of  $J_L$  be equal to this gravity force:

$$|J_L \times B| \sim J_L B \sim 3.2 \times 10^{-11} \text{ erg cm}^{-4}, \quad (11)$$

and for  $B \sim 10 \text{ G}$ ,  $J_L \sim (3.2/8\pi) \times 10^{-12} \text{ G cm}^{-1}$  which implies that  $J_L \sim 10^{-3} \mu\text{A m}^{-2}$  (cf., Priest, 1982, p. 395, eqn 11.30). Here we have used  $1.2 \times 10^{-2} \text{ G m}^{-1} = 1 \text{ A m}^{-2}$  and  $\text{erg cm}^{-3} = \text{G}^2/8\pi$ . This value for  $J_L$  is significantly smaller than  $J_\phi$  estimated above.

The electric currents induced by radial stretching are larger than would be required to overcome the gravity term in the force equation. However, these currents are consistent with those of Bogdan and Low (1986) who showed that a 3D magnetostatic model of the solar corona with a  $1/r^2$  gravity field can be generated analytically with the assumption that the coronal currents be everywhere perpendicular to gravity (i.e. non-radial). This is the identical situation implied by the field transformations of section 2. Consequently, we envisage that the

large Lorentz forces generated by the coronal currents would be balanced primarily by transverse pressure gradients, i.e.  $dp/d\theta$ . Such a model is beyond the scope of the present work, since a proper treatment of an active region atmosphere would require the self-consistent incorporation of an energy equation in addition to the force balance equations.

In the foregoing, we have neglected the possibility of MHD flows providing the necessary force balance. However, a quick calculation suggest that in the absence of substantially enhanced flows the force balance must be dominated by the transverse pressure gradients as stated above. For steady outflows, the equation of motion has the additional term  $nm(\mathbf{v} \cdot \nabla)\mathbf{v}$ . As an estimate of the order of magnitude of this term we use the results of Grall et al. (1996) for polar winds. For a  $500\text{km s}^{-1}$  velocity increase over  $5 r_{\odot}$ , the solar wind effect is on the order of  $1.2 \times 10^{-11} \text{erg cm}^{-4}$  for a mass density of  $\rho = 1.7 \times 10^{-15} \text{g cm}^{-3}$ , comparable to  $|\frac{dp}{dr}| \sim \rho g$

The electric currents required to generate the active region morphology place severe constraints on the forces present in the corona. However, without more understanding of the gradients across the observed loop structures in the active region and the magnitude of the flows within these structures we cannot rule out such large cross-field currents.

We should note that we chose the lower boundary condition for the potential solution to be the observed magnetogram with the tacit assumption of an upper boundary condition of zero field at infinity. In fact, what we have not considered is the possibility that the presence of MHD flows deforms the actual upper boundary condition: a situation which the application of the source-surface models addresses. Hence, in future work we will include a potential, source-surface model to augment the present approach.

## 5. Conclusion

The results of this study are: (1) radially stretching extrapolated potential field lines improves the relationship between the coronal field and the observed soft X-ray structures. (2) The resulting magnetic field is non-force free with non-radial electric currents. Though not shown explicitly, we have determined that a truncated Green's function source-surface model will not provide adequate radial stretching for the region for any source-surface height (Sakurai, 1982). (3) Magneto-static force balance can only be achieved by strong transverse pressure gradients.

We conjecture that the cross-field currents simulate the MHD solar-wind effect where the plasma beta  $\beta = 2\mu p/B^2 \sim 1$ , by altering the

field to simulate a solution with the appropriate upper boundary conditions. In addition, the presence of such non-force-free distributions may yield the necessary ‘latent’ coronal energy for coronal mass ejections, and may be responsible for the energy released in solar flares.

The resulting magnetic field solution provides an important construct to which other analytical and numerical models must comply. We have derived a coronal magnetic model by establishing a magnetic field which yields a set of field lines consistent with the observed coronal loops. However, the initial field was restricted by the use of a potential field extrapolation. The code used to generate the extrapolated field is further restricted in that the locations for conjugate footpoints of a closed coronal field line are fixed. Future extension of the process would incorporate a more general force-free model in which the pair of conjugate foot points can be varied, providing an environment in which a general flux tube could be realized. Increasing the number of variables would allow a better 3D magnetic field solution without loss of information.

### **Acknowledgements**

Part of this work was supported by the NASA Office of Space Science under the space science theme of the Sun-Earth Connection (GAG) and

under contract NAS 8-37334 (DA). We thank S. Suess and R. Moore (MSFC) and S. Gibson (GSFC) for helpful comments and discussions. We wish to thank T. Sakurai for making his potential code available and his assistant in its implementation at MSFC. *Yohkoh* is a mission of the Japanese Institute for Space and Astronautical Science.

## Appendix

### A. Coronal Flux Correlation with Stretched Field Lines

In this Appendix, we establish a quantitative correlation between the observed coronal loops and the extrapolated field lines. The following steps are employed: (1) The coronal loops of a combined set of SXT images for 1996 November 26 are enhanced by an unsharp masking algorithm. (2) Individual loops are delineated and their loci determined (3) The position of the average apex of the coronal loops are compared to the position of the average apex of the stretched field lines for a series of stretching factors. The magnetic field apex is defined as the position of the maximum height of stretched magnetic field lines. The line-of-sight loop apex is defined as the position which has the maximum radial value,  $r_{max}$ , (in 2D) from the centroid of the distribution of longitudinal magnetic field strength. The result is that the stretching

factor of  $k \approx 3.4$  provides the maximum correlation for coronal loops (in the range  $100 < r_{max} < 400$  arcsec or  $0.10r_{\odot} < r_{max} < 0.42r_{\odot}$ )

A set of nine SXT images over a three hour interval were summed after co-registration using a transformation for solar differential rotation (Scherrer, Wilcox, and Svalgaard, 1980). The Yohkoh/SXT AIMg images, shown in Figure 5, were taken over a 3 hour period from 20:36 to 23:41 UT with the first image being the reference image to which all others are co-aligned. The enhancement process of unsharp masking, subtraction of a smoothed version of the image from itself, was applied to the summed images and the result is displayed in Figure 5b. The unsharp masking algorithm uses a Lee Filter which smoothes additive image noise by generating statistics in a local neighborhood and comparing them to expected values (Lee 1986; IDL routine LEEFILT). From the enhanced image 17 coronal loops were easily identified; Figure 5c.

To locate the apexes in the image plane, a polar coordinate system was defined by locating the origin at the centroid of the longitudinal field strength distribution. The polar angle for a line from the origin to an apex is measure from a line parallel to the vector from disk center to the extreme western limb. The magnetic centroid was transformed to the appropriate image coordinates taking into account the time difference between the magnetogram and SXT reference time using the

sidereal differential rotation rate. The magnetic field lines are extrapolated from the KPNO magnetogram and, hence, the magnetic centroid provided a natural origin for the polar coordinates of the field lines for this magnetically simply-configured active region.

The radial apex position for short loops ( $r < 100$  arcsec) can be significantly displaced from an apex as defined by the maximum height for the computed field lines. The angular position of the apex can be shown to be a limiting envelope of the radial apex angles for the computed field lines. Hence, the apex of the field lines is compared with the radial apex of the coronal loops, since the coronal loops show no large distortion that would result from line-of-sight effects; this implies that the coronal loops have a low inclination angle with respect to the tangential plane. The maximum coronal loop apex has a radial value of 351 arcsec from the magnetic centroid. Therefore, we have limited the apex comparison to the radial range 100–400 arcsec. The coronal loops were classified into northern and southern groups since their polar angles are separated by  $\sim 180^\circ$ . The average apex for these two groups is shown in Figure 6. The sign of angular position for the southern groups and field lines have been reversed for this display.

The average height apex in the comparison range is calculated for a set of stretching factors ( $k=1, 2, 3, 3.5, 4, 4.5$ ). A total of 256 unstretched, potential, field lines ( $k=1.0$ ) were calculated using the

Sakurai spherical potential code and the stretching transformation was applied to these field lines (Sakurai, 1982). This distribution of the fieldline footpoints was determined by the code's magnetic flux strength algorithm. The resulting angular coordinate for the average radial apex as a function of the stretching factors is shown in Figure 6. The average apex of the southern set of stretched field lines intercept the value of the average coronal apex at  $k = 4.3$  and the northern set at 2.5 with a mean of  $k = 3.4$ . Hence, field lines with a stretching factor of  $k \simeq 3.4$  best approximate the structure of the active region corona.

### B. Approximation of $J_\phi$

In this Appendix, an approximation to the  $\phi$ -component of the electric current density  $J_\phi$  is derived by approximating the equivalent  $J_x$ . The spherical coordinates are replaced locally with the appropriate Cartesian expressions. For  $J_x$ , we have

$$4\pi J_x = \frac{\partial B'_y}{\partial z} - \frac{\partial B'_z}{\partial y}, \quad (12)$$

and for the potential case,  $k = 1$ ,  $J_x = 0$ . The spatial stretch gives a  $J_x$  value of



$$4\pi J_x = \frac{\partial[v(z, r_\odot, k) B_y]}{\partial z} - \frac{\partial[(kv(z, r_\odot, k))^2 B_z]}{\partial y}, \quad (13)$$

where we have replaced  $w$  by its equivalent,  $w = k^2 v^2$ . Hence

$$4\pi J_x = (v - k^2 v^2) \frac{\partial B_y}{\partial z} + B_y \frac{\partial v}{\partial z} - (k^2 B_z) \frac{\partial v^2}{\partial y} + k^2 v^2 \left[ \frac{\partial B_y}{\partial z} - \frac{\partial B_z}{\partial y} \right], \quad (14)$$

and the last two terms are zero. For  $k \sim 3.4$  and  $z \sim 0.2r_\odot$  then  $\partial v/\partial z = r_\odot(1 - k)/(k(kz + r_\odot)^2) \sim -1/(4r_\odot)$  and  $(v - k^2 v^2) \sim -0.3$ , hence  $|4\pi J_x| \sim 0.3 \partial B_y/\partial z$ . Now  $\partial B_y/\partial z \sim \partial B_z/\partial y \sim B_z(z = 0.2r_\odot)/L$  and  $L = 2.5 \times 10^8$  m is the scale of the active region as measured from the *Yohkoh/SXT* images. Assuming a field strength of 10 G at  $z = 0.2r_\odot$ ,  $|4\pi J_x| \sim 0.3 \times 10 / 2.5 \times 10^8 \sim 1.2 \times 10^{-8}$  G m<sup>-1</sup>  $\sim 10^{-6}$  A m<sup>-2</sup>.

Hence, the  $\phi$ -component of the electric current density  $J_\phi \sim 0.079 \mu\text{A m}^{-2}$

### List of Figures

Figure 1. Transformed field lines in relationship to coronal loop structures as the radial stretching factor is varied from  $k = 1.$ , 1.5, 3.0, to 4.5 for 1996-Nov-26. An arrow is used to draw attention to the evolution of the transformed field lines in the south of the active region which conform to the observed loops as  $k$  is increased.

Figure 2. Transformed field lines in relationship with coronal loop structures for the radial stretching factor  $k = 3.0$  for 1996-Nov 26, 27, 28, and Dec-2 (limb view).

Figure 3. A plot of the magnitude of the magnetic field strength (G) along the potential field lines versus height. For reference the dashed curves are a plot of the empirical functions  $B = 1000 e^{-\zeta \sqrt{h}}$ , where  $\zeta = 1.3, 1.5,$  and  $1.7$ .

Figure 4. The inferred variation of gas pressure and plasma beta with height for AR 7999. A line-of-sight integration path length of  $2.5 \times 10^4$  km was assumed. The median magnetic field was given by the expression of Figure 3:  $B = 1000 e^{-1.5 \sqrt{h}}$ .

Figure 5. Enhancement of the Yohkoh/SXT Image for AR 7999. The three panels show (a) the original summed image of nine Yohkoh/SXT, (b) the enhance coronal loop image using an unsharp masking technique, and (c) the digitized coronal loops using a cursor input and then employing a polynomial fit on the polar coordinates of the points to smooth the curves.

Figure 6. The angular polar coordinates of the average apex position for the average northern (dashed) and southern (solid) field lines as function of the stretching factor. These curves are compared to the average radial apex position for the coronal loops (horizontal lines). The southern (northern) average of the coronal loops of  $-78^\circ$  ( $66^\circ$ ) cor-

responds to stretching of  $k = 4.3(2.5)$ . The mean value of  $k = 3.4$  is the average stretching factor for the entire region.

## References

- Acton, L. W.: 1996, 'Comparison of Yohkoh X-ray and Other Solar Activity Parameters for November 1991 to November 1995', *Proc. of Ninth Coolstar Workshop*, Florence, Italy, 3-6 October 1995.
- Alexander, D.: 1998, 'Temperature Structure of the Quiet X-ray Corona', *J. Geophys. Res.*, in print.
- Altschuler, M. D., and Newkirk, G. Jr.: 1969, 'Magnetic Fields and the Structure of the Solar Corona I: Methods of Calculating the Coronal Fields', *Solar Physics*, **Vol. 9**, pp. 131-149
- Amari, T., Aly, J. J., Luciani, J. F., Boulmezaoud, T. Z., and Mikić, Z.: 1997, 'Reconstructing the Solar Coronal Magnetic Field as a Force-Free Magnetic Field', *Solar Physics*, **Vol. 174**, pp. 129-149
- Antiochos, S. K. and Dahlburg, R. B.: 1997, 'The Implications of 3D for Solar MHD Modeling', *Solar Physics*, **Vol. 174**, pp. 5-19
- Bagenal, F., and Gibson, S. E.: 1991, 'Modeling the large-scale structure of the solar corona', *Journal Geophys. Research*, **Vol. 96**, pp. 17663-17674
- Bogdan, T. J., and Low, B. C.: 1986, 'The three-dimensional structure of magnetic atmospheres II: Modeling the large-scale corona', *Astrophys. Journal*, **Vol. 306**, pp. 271-283
- Grall, R. R., Coles, W. A., KlingleSmith, M. T., Breen, A. R., Williams, P. J. S., Markkanen, J, and Esser, R.: 1996, 'Rapid Acceleration of the Polar Solar Wind', *Nature*, **Vol. 379**, pp. 429-432
- Gary, G. A.: 1990, 'Concerning the Extrapolation of Solar Non-Linear Force-Free Magnetic Fields', *Memorie della Societa Astronomica Italiana*, **Vol. 61**, pp. 457-475
- Gibson, S. E., and Bagenal, F.: 1995, 'The large-scale magnetic field and density distribution in the solar minimum corona', *Journal Geophys. Research*, **Vol. 100**, pp. 19865-19880
- Gibson, S. E., and Low, B. C.: 1998, 'A Time-Dependent Three-Dimensional Magnetohydrodynamic Model of the Coronal Mass Ejection', *Astrophys. Journal*, **Vol. 493**, pp. 460-473
- Hara, H., Tsuneta, S., Lemen, J. R., Acton, L. W., and McTiernan, J. M.: 1992, 'High-temperature plasmas in active regions observed with the Soft X-ray Telescope aboard Yohkoh', *Publ. Astr. Soc. Japan*, **Vol. 44**, pp. L135-L140
- Hiei, E., Hundhausen, A. J.: 1996, 'Development of a Coronal Helmet Streamer of 24 January 1992', in *Magnetodynamic Phenomena in the Solar Atmosphere - Prototypes of Stellar Magnetic Activity*, eds. Y. Uchida, T. Kosugi, and H. S. Hudson, Kluwer Academic Pub., Boston, pp. 125-126
- Jiao, L., McClymont, A. N., and Mikić, Z.: 1997, 'Reconstruction of the Three-Dimensional Coronal Magnetic Field', *Solar Physics*, **Vol. 174**, pp. 311-327
- Lee, X. X.: 1986, 'Speckle Suppression and Analysis for Synthetic Aperture Radar', *Optical Engineering*, **Vol. (25(5))**, pp. 636-646
- Levine, R. H., Schulz, M., and Frazier, E. N.: 1982, 'Simulation of the Magnetic Structure of the Inner Heliosphere by Means of a Non-Spherical Source Surface', *Solar Physics*, **Vol. 77**, pp. 363-392

- McClymont, A. N., Jiao, L., and Mikić, Z.: 1997, 'Problems and Progress in Computing Three-Dimensional Coronal Active Region Magnetic Fields from Boundary Data', *Solar Physics*, **Vol. 174**, pp. 191–281
- Mikić, Z., Barnes, D.C., and Schnack, D.D.: 1988, 'Dynamical Evolution of a Solar Coronal Magnetic Field Arcade', *Astrophys. Journal*, **Vol. 328**, pp. 830–847
- Priest, E. R.: 1972, 'Solar Magnetohydrodynamics', Reidel Pub., New York
- Pneuman, G. W., and Kopp, R. A.: 1972, 'Gas-Magnetic Field Interactions in the Solar Corona', *Solar Physics*, **Vol. 18**, pp. 258–270
- Rosner, R., Tucker, W. H., and Vaiana, G. S.: 1978, 'Dynamics of the Quiescent Solar Corona', *Astrophys. Journal*, **Vol. 220**, pp. 643–665
- Sakurai, T.: 1981, 'Calculation of Force-Free Magnetic Field with Non-Constant  $\alpha$ ', *Solar Physics*, **Vol. 69**, pp. 343–359
- Sakurai, T.: 1982, 'Greens Function Methods for Potential Fields', *Solar Physics*, **Vol. 76**, pp. 301–321
- Sakurai, T.: 1989, 'Computational Modeling of Magnetic Fields in Solar Active Regions', *Space Science Reviews*, **Vol. 51**, pp. 11–48
- Sakurai, T.: 1993, 'Computational Modeling of Solar Magnetic Fields' *Astronomical Society of the Pacific Conference Series*, **Vol. 46**, pp. 91–97
- Schatten, K. H., Wilcox, J. M., and Ness, N. F.: 1969, 'A Model of Interplanetary and Coronal Magnetic Fields', *Solar Physics*, **Vol. 6**, pp. 442–455
- Scherrer, P. H., Wilcox, J. M., and Svalgaard, L.: 1980, 'The Rotation of the Sun: Observations at Stanford' *Astrophys. Journal*, **Vol. 241**, pp. 811–819
- Strong, K. T.: 1994, 'Observations of Structure and Dynamics of Coronal Loops', in *New Look At the Sun with Emphasis on Advance Observations of Coronal Dynamics and Flares*, Proceedings of Kofu Symposium, eds. S. Enome and T. Hirayama, NRO Report No. 360, Nagano, Japan, pp. 53–56
- Suess, S.: 1998, Private Communication
- Tsuneta, S.: 1996, 'Structure and Dynamics of Magnetic Reconnection in a Solar Flare', *Astrophys. J.*, **Vol. 456**, pp. 840–849
- White, S. M., and Kundu, M. R.: 1997, 'Radio Observations of Gyroresonance Emission from Coronal Magnetic Fields', *Solar Physics*, **Vol. 174**, pp. 31–52
- Wolfson, R., and Dlamini, B.: 1997, 'Cross-Field Currents: An Energy Source for Coronal Mass Ejections?', *Astrophysical Journal*, **Vol. 483**, pp. 961–971
- Zhao, X. and Hoeksema, J. T.: 1997, 'Prediction of the Interplanetary Magnetic Field Strength', *J. Geophys. Res.*, **Vol. 100**, pp. 19–33

*Address for correspondence:* G. Allen Gary  
 Space Science Laboratory/ES82  
 NASA/Marshall Space Flight Center, AL 35812, U.S.A.

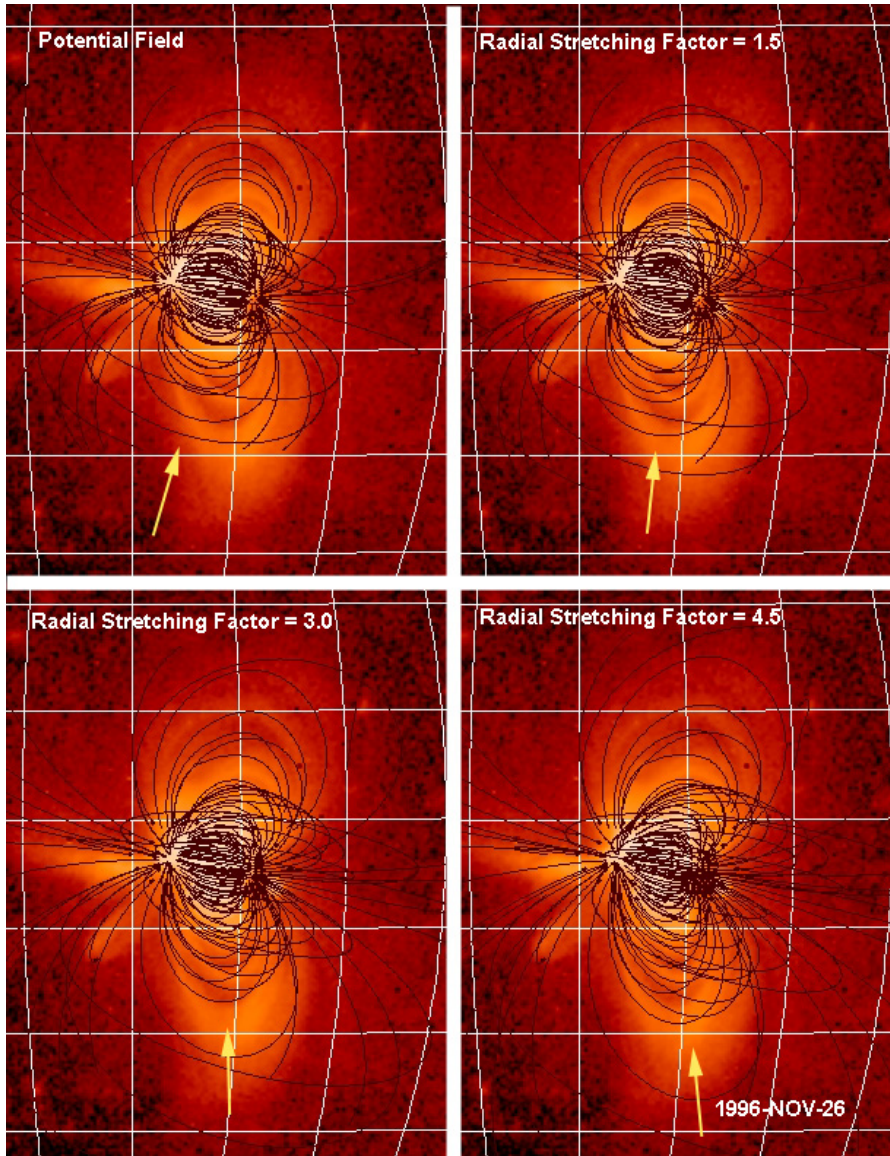


*Figure 1.* Transformed field lines in relationship to coronal loop structures as the radial stretching factor is varied from  $k = 1.$ , 1.5, 3.0, to 4.5 for 1996-Nov-26. An arrow is used to draw attention to the evolution of the transformed field lines in the south of the active region which conform to the observed loops as  $k$  is increased.

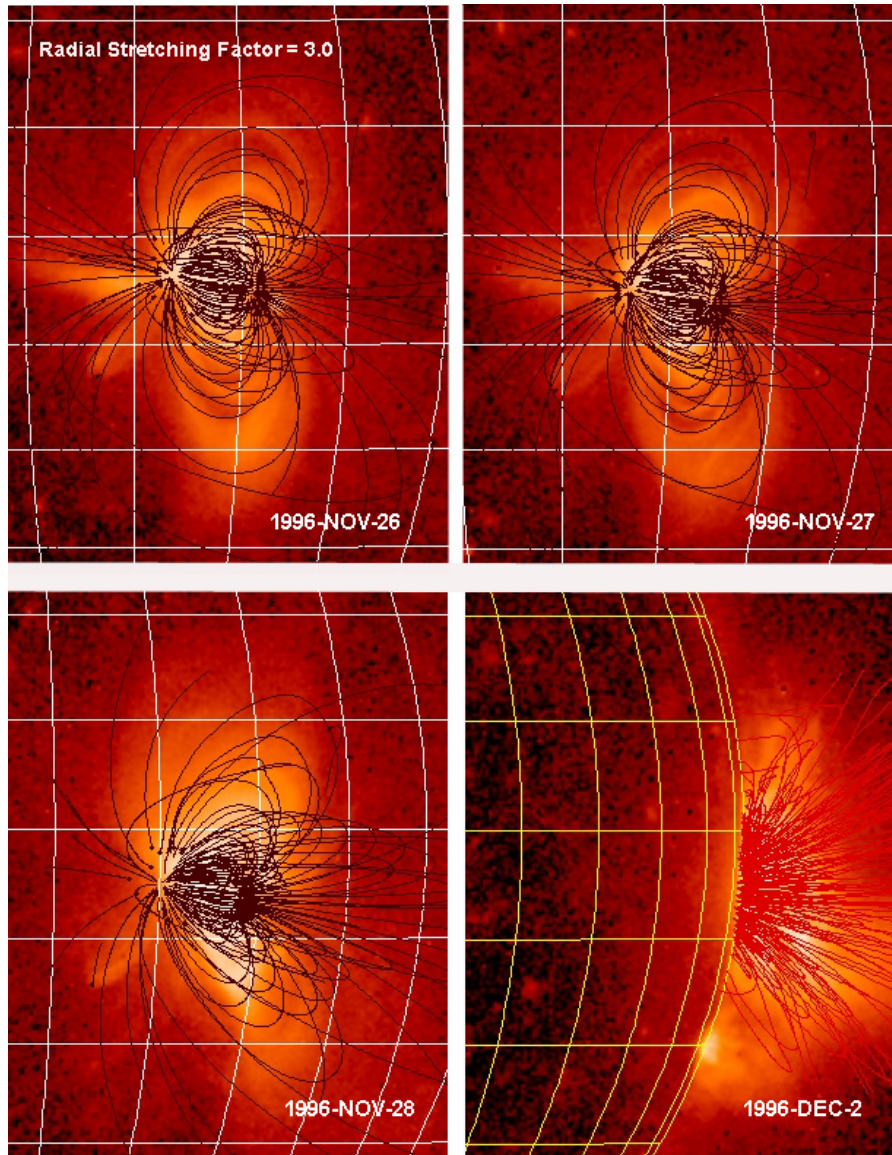


*Figure 2.* Transformed field lines in relationship with coronal loop structures for the radial stretching factor  $k = 3.0$  for 1996-Nov 26, 27, 28, and Dec-2 (limb view).

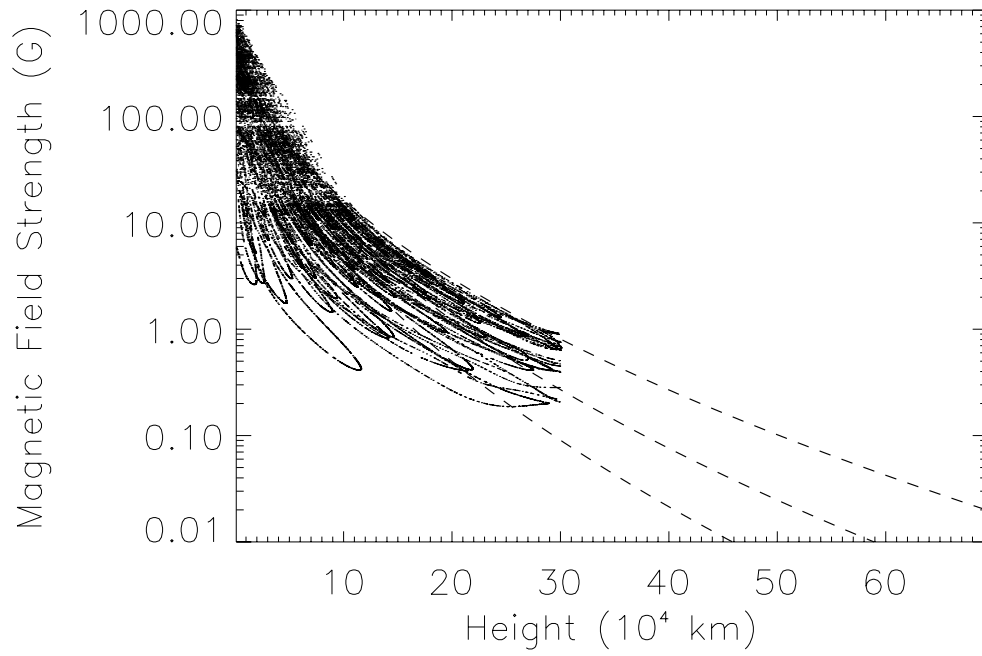


*Figure 3.* A plot of the magnitude of the magnetic field strength (G) along the potential field lines versus height. For reference the dashed curves are a plot of the empirical functions  $B = 1000 e^{-\zeta \sqrt{h}}$ , where  $\zeta = 1.3, 1.5,$  and  $1.7$ .

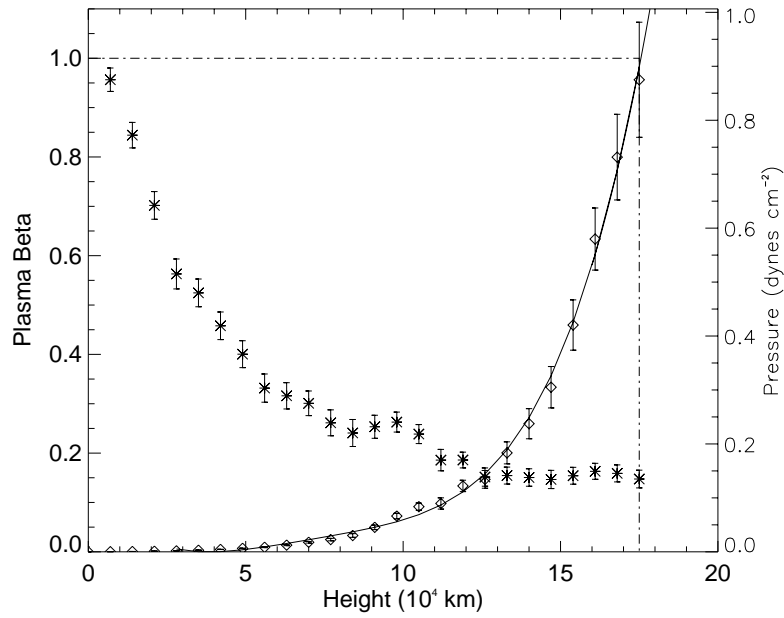
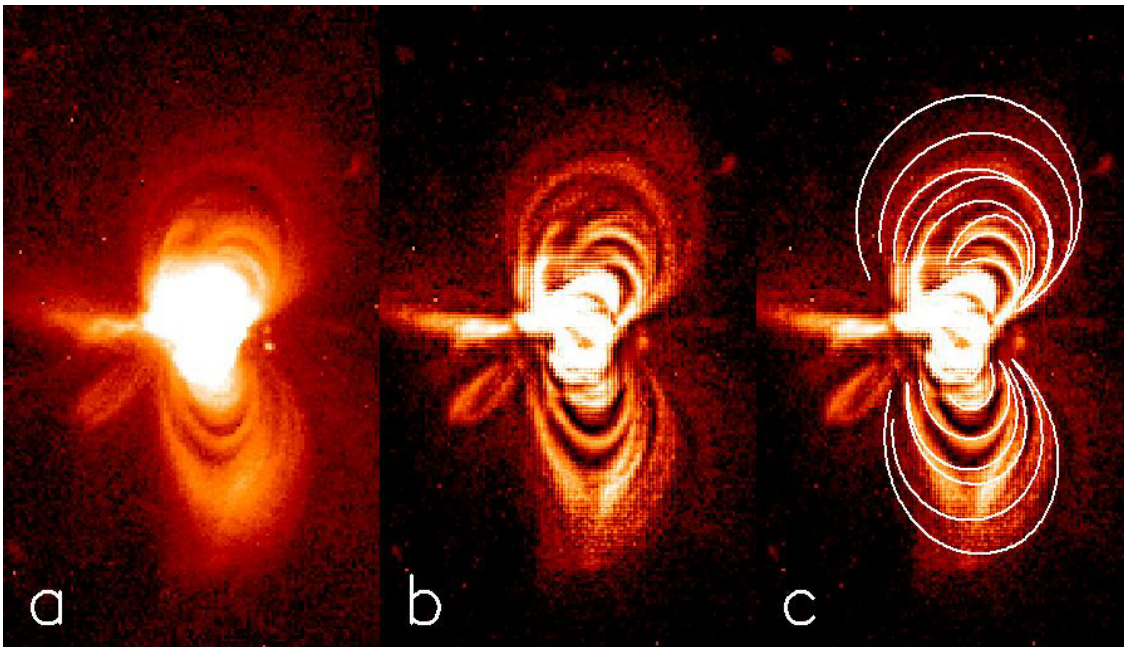
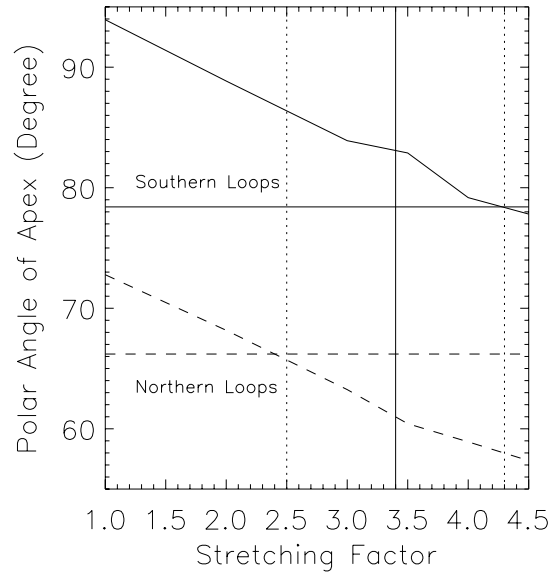


Figure 4. The inferred variation of gas pressure and plasma beta with height for AR 7999. A line-of-sight integration path length of  $2.5 \times 10^4$  km was assumed. The median magnetic field was given by the expression of Figure 3:  $B = 1000 e^{-1.5 \sqrt{h}}$ .





*Figure 5.* Enhancement of the Yohkoh/SXT Image for AR 7999. The three panels show (a) the original summed image of nine Yohkoh/SXT, (b) the enhance coronal loop image using an unsharp masking technique, and (c) the digitized coronal loops using a cursor input and then employing a polynomial fit on the polar coordinates of the points to smooth the curves.



*Figure 6.* The angular polar coordinates of the average apex position for the average northern (dashed) and southern (solid) field lines as function of the stretching factor. These curves are compared to the average radial apex position for the coronal loops (horizontal lines). The southern (northern) average of the coronal loops of  $-78^\circ$  ( $66^\circ$ ) corresponds to stretching of  $k = 4.3$  ( $2.5$ ). The mean value of  $k = 3.4$  is the average stretching factor for the entire region.